Arch Toxicol (2016) 90:2711–2724
DOI 10.1007/s00204-015-1626-2

MOLECULAR TOXICOLOGY

Catalytic efficiencies of directly evolved phosphotriesterase variants with structurally different organophosphorus compounds in vitro

Moshe Goldsmith[2] · Simone Eckstein[1] · Yacov Ashani[2] · Per Greisen Jr.[3] · Haim Leader[4] · Joel L. Sussman[5] · Nidhi Aggarwal[5] · Sergey Ovchinnikov[3] · Dan S. Tawfik[2] · David Baker[3] · Horst Thiermann[1] · Franz Worek[1]

Received: 27 July 2015 / Accepted: 22 October 2015 / Published online: 26 November 2015

Abstract The nearly 200,000 fatalities following exposure to organophosphorus (OP) pesticides each year and the omnipresent danger of a terroristic attack with OP nerve agents emphasize the demand for the development of effective OP antidotes. Standard treatments for intoxicated patients with a combination of atropine and an oxime are limited in their efficacy. Thus, research focuses on developing catalytic bioscavengers as an alternative approach using OP-hydrolyzing enzymes such as *Brevundimonas diminuta* phosphotriesterase (PTE). Recently, a PTE mutant dubbed C23 was engineered, exhibiting reversed stereoselectivity and high catalytic efficiency (k_{cat}/K_M) for the hydrolysis of the toxic enantiomers of VX, CVX, and VR. Additionally, C23's ability to prevent systemic toxicity of VX using a low protein dose has been shown in vivo. In this study, the catalytic efficiencies of V-agent hydrolysis by two newly selected PTE variants were determined. Moreover, in order to establish trends in sequence–activity relationships along the pathway of PTE's laboratory evolution, we examined k_{cat}/K_M values of several variants with a number of V-type and G-type nerve agents as well as with different OP pesticides. Although none of the new PTE variants exhibited k_{cat}/K_M values $>10^7$ M^{-1} min^{-1} with V-type nerve agents, which is required for effective prophylaxis, they were improved with VR relative to previously evolved variants. The new variants detoxify a broad spectrum of OPs and provide insight into OP hydrolysis and sequence–activity relationships.

Keywords Organophosphorus compounds · Organophosphate hydrolase · Phosphotriesterase · Bioscavenger · Mutant · Detoxification

Moshe Goldsmith and Simone Eckstein have contributed equally to this article.

Electronic supplementary material The online version of this article (doi:10.1007/s00204-015-1626-2) contains supplementary material, which is available to authorized users.

✉ Franz Worek
franzworek@bundeswehr.org

[1] Bundeswehr Institute of Pharmacology and Toxicology, Neuherbergstrasse 11, 80937 Munich, Germany

[2] Department of Biological Chemistry, Weizmann Institute of Science, Rehovot, Israel

[3] Institute for Protein Design and Department of Biochemistry, University of Washington, Seattle, WA 98195, USA

[4] Department of Materials and Interfaces, Weizmann Institute of Science, Rehovot, Israel

[5] Department of Structural Biology, Weizmann Institute of Science, Rehovot, Israel

Introduction

Organophosphorus compounds (OPs) induce their toxicity by inhibition of the pivotal enzyme acetylcholinesterase (AChE). This results in accumulation of acetylcholine (ACh) at central and peripheral synapses (Aldridge and Reiner 1972; Marrs 2007) with subsequent overstimulation followed by multiple signs and symptoms, e.g., convulsions, respiratory arrest that leads eventually to death (Grob 1956; Marrs 2007). The widespread use of OP pesticides and the repeated misuse of OP nerve agents as chemical warfare agents emphasize the need for an effective medical treatment. Currently, intoxication by OPs is treated with a combination of atropine (muscarinic antagonist) and oximes (reactivation of inhibited AChE) (Johnson et al. 2000; Thiermann et al. 2013); however, the standard therapy has

limited efficacy depending on the type and dose of OP (Worek and Thiermann 2013).

These disadvantages could be overcome by detoxification of OPs before entering target tissues (Nachon et al. 2013). An extensively investigated option is to use human butyrylcholinesterase (hBuChE), an enzyme which acts as a stoichiometric scavenger and therefore has to be applied in high doses (Ashani and Pistinner 2004; Masson et al. 2009). An increasing focus is put on catalytic bioscavengers, i.e., enzymes that hydrolyze OPs without being consumed and can be applied at low doses (Lenz et al. 2007). Candidates are mammalian paraoxonase (PON1), *Brevundimonas* (formerly *Pseudomonas diminuta*), organophosphate hydrolase (OPH) (also called phosphotriesterase—PTE), *Alteromonas* prolidase, organophosphorus acid anhydrase (OPAA), and *Loligo vulgaris* diisopropylfluorophosphatase (DFPase) (Masson and Rochu 2009).

OP nerve agents are racemic mixtures of the highly toxic P(−) and the less toxic P(+) enantiomer (de Jong and Benschop 1988). Unfortunately, the P(−) enantiomers of nerve agents are barely hydrolyzed by the existing wild-type enzymes due to their stereopreference toward the P(+) enantiomer (Bigley et al. 2013). Previous analysis estimated that effective in vivo detoxification using reasonable enzyme doses (<1 mg kg^{-1} body weight, assuming an enzyme M.W. of ~40 kDa) demands a catalytic efficiency of $>10^7$ M^{-1} min^{-1} for hydrolysis of the toxic P(−) isomers of nerve agents (Gupta et al. 2011). Hence, research efforts are focused on engineering enzymes with high k_{cat}/K_M values as well as P(−) stereopreference.

In addition, V-type nerve agents, e.g., VX, VR, and CVX, present a specific challenge due to their high percutaneous toxicity and long persistence in the human body (Masson et al. 2009). Recently, the engineered phosphotriesterase (PTE) mutant C23 with reversed stereoselectivity was found to hydrolyze the P(−) enantiomers of VX, CVX, and VR with a catalytic efficiency, k_{cat}/K_M, up to 5×10^6 M^{-1} min^{-1} in vitro (Cherny et al. 2013) and was able to prevent systemic toxicity as post-exposure therapy in VX poisoned guinea pigs at low protein dose (Worek et al. 2014b).

In the present study, we describe our attempts to obtain recombinant PTE variants with improved catalytic efficiencies for VX and VR hydrolysis using directed evolution methods. We provide a detailed in vitro analysis of the catalytic activities of two newly selected and four previously selected variants. The activities of these six PTE variants, expressed and purified from *E. coli* cells, with 13 different V-type nerve agents, four G-type nerve agents, and three pesticides are compared with that of the wild-type-like PTE variant S5 (wt-PTE S5) (Roodveldt and Tawfik 2005). From these data, we attempt to explain how OP structure and variant sequence determine its catalytic efficiency of hydrolysis.

Materials and methods

Chemicals and reagents

OP nerve agents (Table 1) were made available by the German Ministry of Defence. Stock solutions (1 or 0.1 % v/v) were prepared in acetonitrile and stored at ambient temperature. OP pesticides (Table 1) were purchased from Dr. Ehrenstorfer GmbH (Augsburg, Germany). Stock solutions (10 % v/v) were prepared in acetonitrile and stored at ambient temperature. OP working solutions were appropriately diluted in TNZ buffer (50 mM TRIS–HCl, pH 8.0, 100 mM NaCl, 10 μM $ZnCl_2$) just before use. 5,5′-dithiobis(2-nitrobenzoic acid) (DTNB) and acetylthiocholine iodide (ATCh) were purchased from Sigma-Aldrich (Taufkirchen, Germany). All other chemicals were purchased from Merck Eurolab (Darmstadt, Germany). Hemoglobin-free human erythrocyte ghosts served as AChE source and were prepared according to (Dodge et al. 1963) with minor modifications (Bierwisch et al. 2014). Restriction enzymes EcoRI-HF, PstI-HF and DpnI, pMAL-c2x expression vector and amylose beads were purchased from New England Biolabs (NEB®). Synthetic oligonucleotides were purchased from Sigma (Israel) Benzonase®nuclease from Novagen. Liquid and solid bacterial growth media were purchased from the Bacteriology Unit (Weizmann Institute of Science, Rehovot, Israel).

Computational library design

A computational model of the active variant from earlier library screens, I_F4, was generated using the starting coordinates from the crystal structure of phosphotriesterase from *Pseudomonas diminuta* with pdb accession code 1HZY (Benning et al. 2001). The substitutions were inserted into the initial structure and minimized using the all-atom energy function in Rosetta (Das and Baker 2008).

To computationally screen substitutions at position C59, chain A of the crystal structure (PDB ID: 1HZY) was used, and models with all 20 amino acids were generated using Rosetta. A computational 2D screen of the positions A203X and D233X was performed using the computational model of I_F4 as the starting model. Three computational models were generated: one apo-structure including the metal site as well as two holo structures with transition states models of VX and VR. All models were

Table 1 Chemical structures of tested OPs

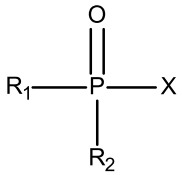

OP	R_1	R_2	X
Dimethyl-VX	Methyl	*O*-ethyl	S-[2-(dimethylamino)ethyl]
VM	Methyl	*O*-ethyl	S-[2-(diethylamino)ethyl]
n-Propyl-VX	Methyl	*O*-ethyl	S-[2-(di-n-propylamino)ethyl]
VX	Methyl	*O*-ethyl	S-[2-(diisopropylamino)ethyl]
CVX	Methyl	*O*-n-butyl	S-[2-(diethylamino)ethyl]
VR	Methyl	*O*-isobutyl	S-[2-(diethylamino)ethyl]
Methyl-VM	Methyl	*O*-methyl	S-[2-(diethylamino)ethyl]
Methyl-VE	Ethyl	*O*-ethyl	S-[2-(dimethylamino)ethyl]
VE	Ethyl	*O*-ethyl	S-[2-(diethylamino)ethyl]
Isopropyl-VE	Ethyl	*O*-ethyl	S-[2-(diisopropylamino)ethyl]
Amiton	*O*-ethyl	*O*-ethyl	S-[2-(diethylamino)ethyl]
Dimethyl-amiton	*O*-ethyl	*O*-ethyl	S-[2-(dimethylamino)ethyl]
Diisopropyl-amiton	*O*-ethyl	*O*-ethyl	S-[2-(diisopropylamino)ethyl]
GA (tabun)	*O*-ethyl	Dimethylamido	CN
GB (sarin)	Methyl	*O*-isopropyl	F
GD (soman)	Methyl	*O*-pinacolyl	F
GF (cyclosarin)	Methyl	*O*-cyclohexyl	F
Malaoxon	*O*-methyl	*O*-methyl	S-(1,2-diethoxycarbonyl)ethyl
Mevinphos	*O*-methyl	*O*-methyl	*O*-(2-methoxycarbonyl-1-methylvinyl)
Chlorpyrifos-oxon	*O*-ethyl	*O*-ethyl	*O*-(3,5,6-trichlorpyridin-2-yl)

visually inspected. For more details, see (Supplementary Materials and Methods).

Co-evolution analysis

To identify individual residues and residue pairs that occurred frequently in naturally occurring family members, we trained a GREMLIN statistical model (Kamisetty et al. 2013) on a set of homologous sequences identified using hhblits (Remmert et al. 2012). Searches were made using the sequence from 1HZY chain A (search parameters are cov 75, id90, reweighted). Substitutions that increased the GREMLIN score by introducing highly conserved residues or residue pairs were then proposed for experimental characterization.

PTE library construction

Libraries of PTE variants were constructed as previously described (Cherny et al. 2013). Briefly, amino acid substitutions were introduced using short oligonucleotides encoding the mutated site flanked by the wild-type sequences. These were added to mixtures of 50- to 250-bp fragments of selected PTE variants, PCR amplified and cloned into a pMAL-c2x expression vector using EcoRI and PstI sites as described in (Rockah-Shmuel et al. 2014). The protocol was tuned to obtain a combinatorial incorporation of the designed mutations at an average of 2 ± 1 mutations per gene.

PTE library screening

Screening was performed as previously described (Cherny et al. 2013). Briefly, randomly picked colonies were individually grown O/N in 96-Deep-Well plates (Axygen®). Overnight cultures were used to inoculate (1:100 dilution) 0.5 ml LB medium with 100 μg/ml ampicillin and 0.1 mM $ZnCl_2$, grown to $OD^{600nm} \approx 0.6$, induced with 0.4 mM IPTG, and grown at R.T O/N. Cells were pelleted and lysed by resuspension and shaking in 300 μl/well of lysis buffer (0.1 M Tris pH 8.0, 0.1 M NaCl, 0.1 % v/v Triton-X100, 0.2 mg/ml lysozyme, 10 mM Na_2CO_3, and 1:50,000 Benzonase nuclease). Lysates were centrifuged and kept at 4 °C O/N before screening. Forty microliters of clear cell lysate from each well were mixed with, 20 μl of in situ generated V-agents

and 50 µl of pure *Tc*AChE (*Torpedo californica* acetylcholinesterase) (final concentrations are given in Supplementary Table 1). The reaction mixtures were incubated for 60 min before determination of residual AChE activity by mixing 20 µl of the reaction mixture with 180 µl PBS containing 0.85 mM DTNB and 0.55 mM acetylthiocholine. Initial velocities of acetylthiocholine hydrolysis were determined at 412 nm using a Powerwave HT spectrophotometer (BioTek®).

Enzyme expression and purification

The recombinant PTE variants (MBP fusion) were purified as follows: The gene was cloned into a pMALc2x expression vector (NEB®) and transformed into *E. coli* BL21/DE3 cells. The culture grew in LB medium including ampicillin overnight at 30 °C. The inoculate was diluted 1:100 into LB medium with ampicillin (100 µg/ml) and 0.2 mM $ZnCl_2$ and grown at 30 °C to $OD_{600nm} \approx 0.6$. IPTG was added (0.4 mM), and the culture was allowed to grow overnight at 20 °C. Cells were harvested by centrifugation and resuspended in lysis buffer (0.1 M Tris pH 8.0, 0.1 M NaCl, 10 mM $NaHCO_3$, 1:500 diluted protease inhibitor cocktail (Sigma®), 50 Units Benzonase nuclease, 0.1 mM $ZnCl_2$). Cells were then lysed using sonication, clarified by centrifugation (20,000 rpm, 4 °C, 30 min), and passed through a column packed with amylose beads (NEB®) pre-equilibrated with buffer A (0.1 M Tris pH 8.0, 0.1 M NaCl). Following an extensive wash with buffer A, the MBP–PTE fusion proteins were eluted with buffer A containing 10 mM maltose. The fractions containing pure MBP–PTE variants were pooled and dialyzed over night at 4 °C with buffer A supplemented with zinc (50 mM Tris pH 8.0, 100 mM NaCl and 200 µM $ZnCl_2$). Protein concentrations were examined by absorbance at 280 nm (extinction coefficient value for the MBP fused enzymes was $\varepsilon = 95{,}925$ OD/M).

PTE C23 was prepared in TNZ buffer and stored at −80 °C until use. PTE A53, IV-A1, IV-H3, B141, RD1-G83, wt-PTE S5 were prepared in a modified TNZ buffer (50 mM TRIS–HCl, pH 8.0, 100 mM NaCl, 200 µM $ZnCl_2$), stored at −80 °C, and were diluted 20-fold in TRIS-NaCl pH 8.0 before use.

Enzyme activity determinations

Human AChE activity was measured spectrophotometrically with a modified Ellman assay (Ellman et al. 1961; Worek et al. 1999) at 412 nm and 37 °C (UVmc^2, SAFAS Monaco) using polystyrol cuvettes (VWR®, Darmstadt, Germany). The assay mixture (3.16 ml) contained 0.45 mM ATCh as substrate and 0.3 mM DTNB as chromogen in 0.1 M phosphate buffer (pH 7.4).

Table 2 Final OP concentrations during incubation with PTE

[OP] (µM)	OP
5	VX, VR, CVX, VM, GF
6.7	Isopropyl-VE
10	n-Propyl-VX, VE
12.5	GD
13.3	GB
16.7	Dimethyl-VX, methyl-VM
20.8	GA
25	Methyl-VE
66.7	Diisopropyl-amiton
83.3	Amiton, dimethyl-amiton
166.67	Malaoxon, mevinphos
250	Chlorpyrifos-oxon

Detoxification of OPs by PTEs

The detoxification of OP by PTE variants was investigated with an AChE inhibition assay, using human erythrocyte ghosts as AChE source (Worek et al. 2014a). Nerve agents, pesticides, and PTE variants were appropriately diluted in TNZ buffer (50 mM Tris–HCl pH 8.0, 100 mM NaCl, and 10 µM $ZnCl_2$). 100 µl PTE was mixed with 500 µl OP dilution, resulting in the final concentrations shown in Table 2, and were incubated at 37 °C. At defined time points, 50-µl samples were transferred to a pre-warmed (37 °C) polystyrol cuvette that previously had been filled with 3000 µl phosphate buffer (0.1 M; pH 7.4), 100 µl DTNB (10 mM), and 50 µl ATCh (28.4 mM). Immediately, thereafter, 10 µl AChE was added, and AChE inhibition curves were recorded for 5 min (chlorpyrifos-oxon, CVX, dimethyl-VX, GA, GB, GD, GF, isopropyl-VE, methyl-VE, methyl-VM, n-propyl-VX, VE, VM, VR, and VX) or 20 min (amiton, diisopropyl-amiton, dimethyl-amiton, mevinphos, and malaoxon). All experiments were performed at 37 °C ($n = 4$) at the Bundeswehr Institute of Pharmacology and Toxicology, Munich, Germany, unless specified otherwise.

Data analysis

The recorded AChE inhibition curves were analyzed by non-linear regression analysis to determine the first-order inhibition rate constant k_1 (Aurbek et al. 2006). Then, k_1 was plotted against incubation time of the OP with the PTE (Fig. 1), to calculate the first-order degradation constant k_{obs}. With k_{obs} and the enzyme concentration [E], the ratio of k_{cat} to K_M was determined according to Eq. (1) (Dawson et al. 2008).

$$\frac{k_{cat}}{K_M} = \frac{k_{obs}}{[E]} \quad (1)$$

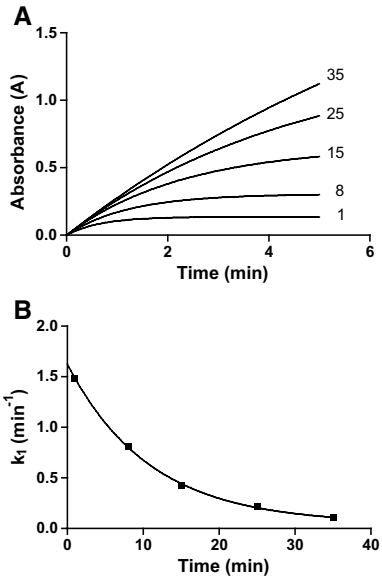

Fig. 1 Time-dependent detoxification of VR by C23. **a** Original registration of the time-dependent (1–35 min) decrease in AChE inhibition by VR after incubation with C23. **b** Secondary graph of k_1 versus time for determination of the detoxification velocity k_{obs}

The second-order rate constant (k_{cat}/K_M) is a comparator for the relative efficiency of PTE against the different OPs. The higher the turnover number (=high k_{cat}) and the higher the affinity of PTE for an OP as substrate (=low K_M), the higher is this ratio. Similar to (Dawson et al. 2008) who observed a linear relationship between k_{cat}/K_M and k_{obs} under a range of enzyme concentrations, the value for k_{obs}/[E] was used here as a reasonable approximation of k_{cat}/K_M.

The analysis of the data and the calculation of the kinetic constants by nonlinear regression analysis were performed with GraphPad Prism 5.0 (GraphPad, San Diego, USA). The data are given as mean ± SD. Differences in catalytic efficacies between C23 and the other PTE variants were analyzed by one-way ANOVA followed by Bonferroni's multiple comparison test. $p < 0.05$ was considered to be statistically significant.

Results

Directed evolution of PTE for VX and VR hydrolysis

Evolved PTE variants C23 and A53 were obtained following five rounds of directed evolution and screening for VX and VR hydrolysis as previously described (Cherny et al. 2013). However, their catalytic efficiencies (k_{cat}/K_M) with V-agents were lower than the desired level of $\geq 10^7$ M^{-1} min^{-1} that is required for efficient in vivo antidotal activity using low protein drug doses (Gupta et al. 2011). In order to improve their activity with the two major V-type threat agents, VX and VR, we generated new libraries of mutants and screened them for VX and VR hydrolysis. Library 6-1 was obtained by shuffling eight variants with different mutational compositions (Supplementary Table 2) that were selected from the previous round 5 of evolution described in (Cherny et al. 2013). They were chosen due to their abilities to efficiently hydrolyze either VX, VR or both agents, in addition to having a diverse mutational composition (e.g., three different residues at positions 59, 106, 203 and four different residues at position 233—Supplementary Table 2). This strategy of library making aimed to combine beneficial mutations that were acquired in separate variants and/or eliminate deleterious mutations from individual variants and was previously employed successfully in the directed evolution of serum Paraoxonase 1 to hydrolyze G-type nerve agents (Goldsmith et al. 2012). Library 6-2 was obtained by shuffling the most active variants selected from round 5 (i.e., A53, C23, and G23) with oligonucleotides encoding for specific substitutions at positions 270 and 273 (Supplementary Table 3). An examination of the computational model that guided the engineering of C23 (Cherny et al. 2013) (Supplementary Fig. 1) suggested these positions may interact with the leaving groups of VX and VR. Thus, the choice of substituting amino acids aimed to replace the small Alanine and Glycine residues at these positions with larger, polar or negative ones (Supplementary Table 3b) in order to improve substrate binding. We screened 420 naïve clones from each library using VX and VR and identified six variants from library 6-1 and nine variants from library 6-2 that, in the cell lysate screening assay, were improved two- to fourfold at VX and VR hydrolysis relative to C23 (materials and methods, Supplementary Table 4). Of these variants, the five most active were purified (Supplementary Fig. 2), and their activity with VX and VR was assayed (Supplementary Table 5). The most improved variant with VR, IVH3, contained a substitution of A270E and was analyzed in detail (Results "Directed evolution of PTE for VX and VR hydrolysis" section).

The modest improvements in activity of round 6 selected variants prompted us to generate and screen additional libraries. Library 7-1 was generated by shuffling variants A53 and G23 while substituting the wild-type Leu residue at position 271 with polar and charged residues (Supplementary Table 6). The two template variants, A53 and G23, were chosen for having the I106A mutation previously shown to enhance efficiency with VR (Cherny et al. 2013). Position 271 was chosen for diversification using the same rational previously employed in choosing position 270. Library 7-2 was generated by shuffling 12 variants selected

from round 6 (Supplementary Table 7a) with oligonucleotides encoding for specific substitutions in nine positions. The choice of the most active variants identified in the previous round of directed evolution as templates for making the next library of variants builds on the idea of gradual improvement in activity. By incrementally accumulating beneficial mutations in each round of selection, we hoped to eventually obtain an enzyme with the required catalytic efficiency. The choice of positions for diversification and the substituting residues in this library was done using both computational and rational designs. From a GREMLIN co-evolution analysis (see Methods), where each position was analyzed to find its evolutionary most optimal pair, the three highest-ranking positions (K77, S258, T350) were selected for substitution. Using a computational model of one of the best variants selected in round 6 (I-F4), docked with the transition-state model of VR, we choose six other positions for substitution (C59, A203, D233, S267, L272, V310). These active-site positions were in close contact with the docked TS model, and their substitution was hypothesized to increase substrate binding and catalysis. The choice of substituting residues at positions 59, 203, 233, and 267 was based on the lowest computed energy scores, while substitutions at 272 and 310 were chosen by a visual analysis of the TS model (Supplementary Materials and methods, Supplementary Table 7b–d).

Since library 7-1 contained only 12 single-residue substitutions on the background of two single variants, screening of ~170 clones from that library with VX and VR was sufficient to cover ~90 % its diversity. In contrast, the diversity of library 7-2 was much greater ($>4\times10^7$). We screened ~500 randomly chosen clones, each containing on average 2 ± 1 mutations, and ~200 clones, each containing on average 4 ± 1 mutations from that library using VX and VR. The idea behind the construction and screening of two versions of this library, which differ in the average number of substitutions per gene, was that a larger number of mutations per variant would increase the chances of

Table 3 Catalytic efficiencies of PTE variants with phosphonothionate V-type nerve agents

OP	k_{cat}/K_M ($\times10^4$ M^{-1} min^{-1} ± SD)						
	C23	A53	IV-A1	IV-H3	B141	RD1-G83	wt-PTE S5
Dimethyl-VX	157 ± 6[a]	32.1 ± 3.5[c]	151 ± 19[g]	46.1 ± 1	1.13 ± 0.05	2.11 ± 1.40	0.27 ± 0.01
VM	402 ± 15[b]	80.2 ± 11.7[c]	282 ± 7[h]	80.2 ± 3.2	10.1 ± 0.2	1.23 ± 0.52	0.7 ± 0.03
n-Propyl-VX	144 ± 1[a]	20.1 ± 1.22[d]	112 ± 6[g]	52.7 ± 8.4	5.61 ± 0.53	2.10 ± 1.19	0.47 ± 0.03
VX	595 ± 16[a]	186 ± 7[e]	253 ± 11[h]	104 ± 1	20 ± 1.06	4.08 ± 0.38	1.02 ± 0.1
CVX	67.5 ± 2.7[a]	185 ± 30.9[f]	305 ± 12[h]	157 ± 8	0.74 ± 0.16	1.20 ± 0.04	0.12 ± 0.04
VR	44.6 ± 1[a]	139 ± 16.6[d]	527 ± 16[h]	149 ± 10	0.75 ± 0.21	0.95 ± 0.05	0.09 ± 0.01
Methyl-VM	28 ± 1[a]	16.6 ± 0.46[c]	43.1 ± 0.6[g]	21.3 ± 2.1	0.59 ± 0.08	0.59 ± 0.03	0.27 ± 0.02
Methyl-VE	403 ± 10[b]	61.6 ± 3.5[c]	424 ± 19[h]	131 ± 12	6.81 ± 0.13	4.02 ± 0.24	0.48 ± 0.04
VE	814 ± 22[b]	204 ± 41[f]	695 ± 47[h]	360 ± 19	32.0 ± 1.47	11.8 ± 0.42	1.28 ± 0.16
Isopropyl-VE	741 ± 55[b]	434 ± 8.8[f]	767 ± 56[h]	502 ± 38	84.7 ± 1.49	14.3 ± 0.67	3.48 ± 0.21

Values are given as mean ± SD ($n = 4$)

PTE concentrations (M) used during incubation with OP: C23 [a] 2.14×10^{-7}, [b] 2.14×10^{-8}; A53. [c] 1.55×10^{-7}, [d] 13.11×10^{-8}, [e] 4.44×10^{-8}, [f] 6.21×10^{-8}; IV-A1, [g] 8.83×10^{-8}, [h] 4.42×10^{-8}; IV-H3 1.42×10^{-7}; B141 1.82×10^{-7}; RD1-G83 1.80×10^{-7}; wt-PTE S5 2.61×10^{-7}

Table 4 Catalytic efficiencies of PTE variants with amiton analogues

OP	k_{cat}/K_M ($\times10^4$ M^{-1} min^{-1} ± SD)						
	C23	A53[c]	IV-A1[c]	IV-H3[c]	B141[c]	RD1-G83[c]	wt-PTE S5[c]
Dimethyl-amiton	7.83 ± 0.65[a]	0.74 ± 0.02	1.02 ± 0.05	1.01 ± 0.09	1.17 ± 0.27	0.3 ± 0.08	0.06 ± 0.01
Amiton	8.19 ± 0.49[a]	3.45 ± 0.16	26.5 ± 6.8	1.43 ± 0.04	0.71 ± 0.05	0.37 ± 0.02	0.21 ± 0.02
Diisopropyl-amiton	14.7 ± 0.7[b]	2.12 ± 0.38	6.5 ± 0.18	5.79 ± 0.51	1.97 ± 0.13	1.28 ± 0.23	0.27 ± 0.00

Values are given as mean ± SD ($n = 4$)

PTE concentrations (M) used during incubation with OP: C23, [a] 2.14×10^{-7}, [b] 1.07×10^{-7}; A53, [c] 1.55×10^{-7}; IV-A1 2.21×10^{-7}; IV-H3 1.42×10^{-7}; B141 1.82×10^{-7}; RD1-G83 1.80×10^{-7}; wt-PTE S5 2.61×10^{-7}

Table 5 Catalytic efficiencies of PTE variants with G-type nerve agents

OP	k_{cat}/K_M ($\times 10^4$ M^{-1} min^{-1} ± SD)						
	C23	A53	IV-A1	IV-H3	B141	RD1-G83	wt-PTE S5
GA	5340 ± 80^{b}	7130 ± 770^{e}	1920 ± 40^{h}	1640 ± 80^{k}	4310 ± 242^{n}	920 ± 33.4^{p}	$20{,}300 \pm 1800^{t}$
GB	5030 ± 600^{a}	1300 ± 280^{c}	2000 ± 60^{h}	684 ± 30^{j}	1530 ± 51.4^{m}	1000 ± 57^{q}	646 ± 73^{s}
GD	264 ± 16^{b}	62.2 ± 4.4^{d}	153 ± 5^{g}	34.1 ± 2.4^{i}	21.6 ± 1.2^{l}	97.9 ± 1.2^{o}	9.94 ± 0.54^{r}
GF	174 ± 23^{b}	278 ± 54^{d}	186 ± 18^{f}	72.4 ± 2.4^{j}	57.4 ± 7.62^{l}	40.4 ± 3.8^{o}	12.4 ± 0.9^{r}

Values are given as mean ± SD ($n = 4$)

PTE concentrations (M) used during incubation with OP: C23, [a] 2.14×10^{-7}, [b] 2.14×10^{-8}; A53, [c] 1.55×10^{-7}, [d] 6.21×10^{-8}, [e] 3.11×10^{-9}; IV-A1 [f] 2.21×10^{-7}, [g] 8.83×10^{-8}, [h] 8.83×10^{-9}; IV-H3, [i] 1.42×10^{-7}, [j] 2.84×10^{-8}, [k] 5.67×10^{-8}; B141, [l] 1.82×10^{-7}, [m] 7.26×10^{-9}, [n] 7.26×10^{-10}; RD1-G83, [o] 1.80×10^{-7}, [p] 3.60×10^{-9}, [q] 7.21×10^{-9}; wt-PTE S5 [r] 2.61×10^{-7}, [s] 1.04×10^{-8}, [t] 1.04×10^{-8}

Table 6 Catalytic efficiencies of PTE variants with OP pesticides

OP	k_{cat}/K_M ($\times 10^4$ M^{-1} min^{-1} ± SD)						
	C23	A53	IV-A1	IV-H3	B141	RD1-G83	wt-PTE S5
Chlorpyrifos-oxon	$144{,}000 \pm 1450^{c}$	$75{,}400 \pm 548^{f}$	$60{,}000 \pm 2170^{i}$	$11{,}300 \pm 73.7^{l}$	$49{,}900 \pm 7980^{o}$	$12{,}500 \pm 483^{r}$	$28{,}700 \pm 1380^{u}$
Malaoxon	1.01 ± 0.04^{a}	1.17 ± 0.06^{d}	0.57 ± 0.05^{g}	1.04 ± 0.04^{j}	1.40 ± 0.06^{m}	1.45 ± 0.06^{p}	1.20 ± 0.07^{s}
Mevinphos	219 ± 27^{b}	48.8 ± 1.17^{e}	30.1 ± 0.75^{h}	24.7 ± 0.42^{k}	87.4 ± 4.41^{n}	30.7 ± 12.5^{q}	119 ± 10.7^{t}

Values are given as mean ± SD ($n = 4$)

PTE concentrations (M) used during incubation with OP: C23, [a] 1.07×10^{-6}, [b] 2.14×10^{-8}, [c] 1.07×10^{-10}; A53 [d] 1.55×10^{-7}, [e] 1.24×10^{-8}, [f] 6.21×10^{-11}; IV-A1 [g] 2.21×10^{-7}, [h] 1.77×10^{-8}, [i] 1.80×10^{-10}; IV-H3, [j] 1.42×10^{-7}, [k] 2.84×10^{-8}, [l] 9.50×10^{-11}; B141 [m] 1.82×10^{-7}, [n] 3.63×10^{-8}, [o] 1.45×10^{-10}; RD1-G83, [p] 1.80×10^{-7}, [q] 1.44×10^{-8}, [r] 2.40×10^{-10}; wt-PTE S5, [s] 2.61×10^{-7}, [t] 1.04×10^{-8}, [u] 2.09×10^{-10}

altering catalytic efficiency but may result in lower protein stability and vice versa. After screening this library using VX and VR, we identified 48 variants improved at VX only (16), VR (11) only, or both (21). We sequenced the eight best variants from each category and also eight variants that had lost their activity with both substrates (Supplementary Table 8). Selected variants were found to incorporate new substitutions at 7 of the nine positions targeted for mutagenesis. The only positions that were not mutated in selected variants were 77 and 272. However, the latter were substituted by only one residue, differing greatly in physical and chemical properties from the original one. The most improved variant at hydrolyzing both VX and VR, IVA1, was purified and subjected to a comprehensive analysis of its catalytic activities with 20 different OPs (Tables 3, 4, 5, 6). This variant, differing from C23 at four positions and from A53 at six positions (Table 7), was similar to C23 in catalytic efficiencies with most substrates. However, it was improved by 4.5-fold and 12-fold with CVX and VR with respect to C23 and by 1.6-fold and 3.8-fold with respect to A53, the best VR hydrolyzing variant we had so far (Cherny et al. 2013). The variant contained two mutations, C59 M and I106A, which according to the computational model is the site of the enzyme that accommodates the larger O-alkyl groups of VR and CVX.

In vitro efficiency of PTE variants

The detoxification of a broad spectrum of OP nerve agents and pesticides (Table 1) by different PTE variants was investigated using an AChE inhibition assay. Each PTE mutant was incubated with appropriate OP concentrations (Table 2). After defined time points, aliquots were transferred into cuvettes to measure AChE inhibition curves, which were quantified by the calculation of the first-order inhibition rate constant k_1 (Fig. 1a). From these data, the first-order detoxification constants k_{obs} were calculated (Fig. 1b). Finally, the catalytic efficiency of the respective PTE was quantified by calculating k_{cat}/K_M (Eq. 1).

Detoxification of V-type nerve agents by PTE variants

As mentioned above, C23 was the most efficient VX hydrolyzing PTE variant we obtained prior to this work. For this reason, we used it as a standard for comparison during the evaluation of both older and newer variants (Figs. 2, 3). C23 hydrolyzed the tested V-type nerve agents with k_{cat}/K_M values ranging from 1.5×10^5 to 6×10^6 M^{-1} min^{-1}. The only exceptions were amiton and its derivatives with k_{cat}/K_M values of 8×10^4 (Tables 3, 4). Other evolved PTE variants were also more active with the phosphonothionates, i.e., VX analogues, hydrolyzing

Table 7 Mutational composition of variants analyzed in this work

Selection round	7	6	5	5	2	1	0
Amino acid	IV-A1	IV-H3	C23	A53	B141	RD1-G83	wt-PTE S5
59	M	C	C	C	C	C	C
77	A	A	A	A	A	K	K
80	V	V	V	V	V	A	A
106	A	A	I	A	I	I	I
132	E	E	E	E	D	F	F
173	N	N	N	Q	T	T	T
203	A	A	A	F	A	A	A
204	A	A	A	A	G	A	A
208	D	D	D	D	D	G	G
233	G	D	D	D	D	D	D
254	G	G	G	G	N	N	H
266		A	A	A	A	A	A
270	A	E	A	A	A	A	A
274	N	I	N	N	S	I	I
319	S	S	S	S	S	R	S
342	S	P	S	P	P	P	P

Variant names and the round in which they were selected are listed on the top rows. Mutations in variants are listed relative to the sequence of wt-PTE S5 whose sequence is listed on the right column. Spaces denote a deleted amino acid

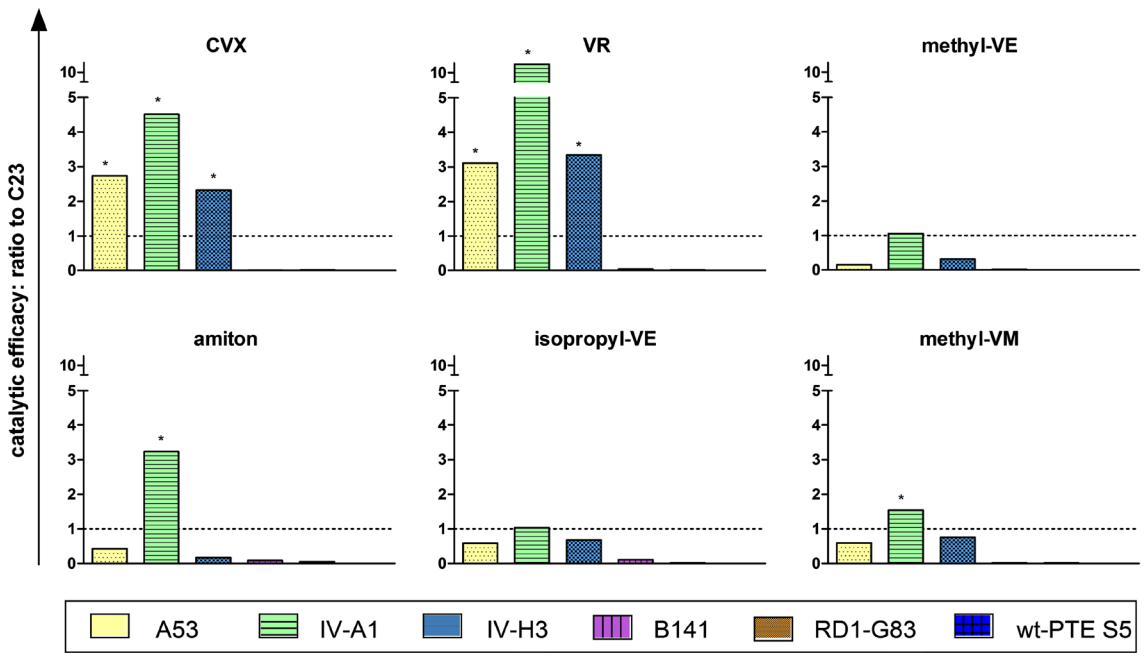

Fig. 2 Catalytic efficiency of PTE variants A53, IV-A1, IV-H3, B141, RD1-G83, and wt-PTE S5 in ratio to C23 (=1, *dotted line*) with CVX, VR, methyl-VE, amiton, isopropyl-VE, and methyl-VM are shown. $^{*}p < 0.05$

them with k_{cat}/K_M values up to ~8×10^6 M^{-1} min^{-1} compared to the tested amiton derivatives. The only exception was IV-A1 with amiton ($k_{cat}/K_M \sim 3 \times 10^5$ M^{-1} min^{-1}; Table 4). In contrast, the catalytic efficiency of wild-type rePTE was substantially lower with these substrates, i.e., k_{cat}/K_M values between 10^2 and 10^4 M^{-1} min^{-1} (Tables 3, 4). PTE variant IV-A1 exhibited significantly higher k_{cat}/K_M values compared to C23 with CVX, VR, amiton, and methyl-VM (Fig. 2). In addition, A53 and IV-H3 hydrolyzed CVX and VR significantly faster than C23 (Fig. 2).

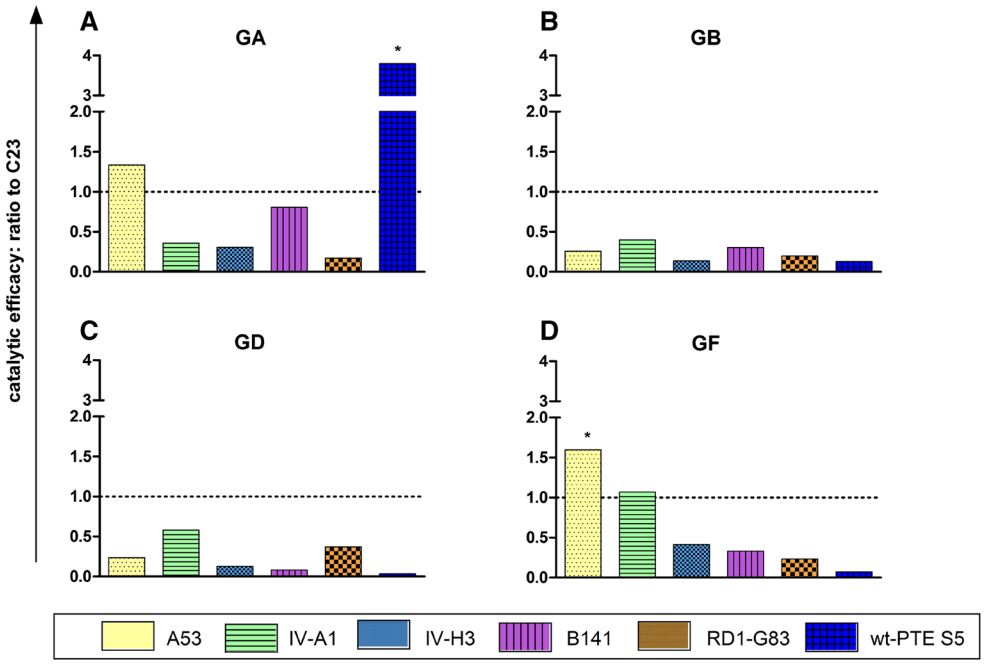

Fig. 3 Catalytic efficiency of PTE variants A53, IV-A1, IV-H3, B141, RD1-G83, and wt-PTE S5 in ratio to C23 (=1, *dotted line*) with GA, GB, GD, and GF are shown. *$p < 0.05$

Detoxification of G-type nerve agents by PTE variants

The tested PTE variants exhibited medium to high catalytic efficacies with G-type nerve agents, i.e., k_{cat}/K_M values between 10^5 and 10^7 M^{-1} min^{-1} (Table 5). They were improved relative to wild-type PTE with all G-agents except GA, for which wild-type PTE showed a high k_{cat}/K_M value of 2×10^8 M^{-1} min^{-1} (Table 5; Fig. 3). All PTE variants exhibited lower catalytic efficiencies with G-agents that have bulky alkyl side chains (GD and GF). Only A53 showed a significantly higher catalytic efficiency compared to C23 with one G-agent (GF; Fig. 3).

Detoxification of OP pesticides by PTE variants

In addition to chemical warfare agents, the detoxification of one selected OP pesticide (mevinphos) and two toxic metabolites of the pesticides malathion and chlorpyrifos (i.e., malaoxon and chlorpyrifos-oxon) by PTE variants was investigated.

All PTE variants had a low to moderate hydrolytic efficiency with malaoxon and mevinphos, respectively (Table 6). However, all PTE variants exhibited high k_{cat}/K_M values, up to 10^9 M^{-1} min^{-1}, with chlorpyrifos-oxon (Table 6).

Factors influencing the measurement of catalytic efficiencies of PTE variants

When we compared the values of catalytic efficiencies of wt-PTE S5, C23, and A53 for different OPs obtained in this work with previous measurements taken in (Cherny et al. 2013), we found differences that ranged between 0.75- and threefold for most OPs. However, greater differences were obtained upon comparing the activities of these variants with amiton and diisopropyl-amiton (i.e., three- to 14-fold). In order to understand the origins of these differences, we repeated the measurements for amiton and diisopropyl-amiton hydrolysis with variants C23 and A53 at different zinc concentrations and at two temperatures (Supplementary Table 9). The repeated measurements uncovered several factors that influenced the determination of catalytic efficiency values: First, the activities of C23 and A53 were inhibited at high zinc concentrations. Catalytic efficiency rates at low zinc concentrations (0.5 μM) such that were used in (Cherny et al. 2013) were up to 2.5-fold greater than rates at higher zinc concentrations (12 μM), similar to the ones used in this work. The inhibition constant (Ki) for C23 with $ZnCl_2$ (4.4 ± 0.09 μM) was found to be lower than the 10 μM $ZnCl_2$ concentration used in this work (data not shown). Thus, despite an essential metal ion for catalytic activity, high zinc ion concentrations can inhibit the activity of PTE variants. Other factors influenced the determination of catalytic rates for the same variants in different laboratories related to differences in protein purity, handling, assay temperature, and experimental setups. For example, while the assays of (Cherny et al. 2013) were done at 25 °C, current values were determined at 37 °C. We found that the acceleration in reaction rates at 37 °C was compromised, in some cases, by a concomitant reduction in the concentration of soluble and active protein in the assay due to reduced thermostability of some variants. Thus, the differences between previous (Cherny et al. 2013) and

current catalytic efficiency values of wt-PTE S5, C23, and A53 relate mainly to the accumulated effects of the different experimental setups used and the final concentration of zinc ions in the reaction.

Discussion

Our initial characterization of PTE variant C23 with different OPs indicated that it was able to hydrolyze V-type nerve agents with k_{cat}/K_M values up to 5×10^6 M^{-1} min^1, and that VX was its best V-type substrate (Cherny et al. 2013). In order to obtain PTE variants with improved catalytic efficiencies, we constructed and screened additional libraries of mutants using both VX and VR. After screening two libraries (6-1, 6-2), we identified five variants improved at VR hydrolysis relative to C23, sequenced and purified them (Table 8). All variants contained the I106A substitution, which according to our computational model is responsible for better active-site accommodation of the large O-alkyl groups of VR and CVX (Table 1) and may also be responsible for the lower activity with the smaller O-alkyl containing substrate—VX. The two best variants isolated, IVH3 and I-F4 (Table 8), also contained an A270E substitution and were improved ~twofold relative to C23 with VR. The most improved variant, IVH3, was subjected to a comprehensive analysis with 18 additional OPs (Tables 3, 4, 5, 6). This analysis revealed that the activities of IVH3 are similar to those of the previously isolated variant A53 (Cherny et al. 2013) apart from its improved efficiencies with VE (~1.8-fold) and Me-VE (twofold). The latter may reflect better binding of small *N*,*N*-dialkyl moieties (i.e., methyl or ethyl) of the leaving groups by the E270 containing IVH3, relative to the A270 containing A53. This effect was more pronounced in VE-like substrates than in VX or amiton-like substrates with similar leaving groups due to different accommodation of the phosphonate moiety of the substrates.

The identification of improved variants that had incorporated mutations at position 270 prompted us to continue and explore this part of PTE. Thus, in the subsequent round of directed evolution, we constructed library 7-1 by mutating position 271 in variants A53 and G23 (Supplementary Table 6). We discovered that different substitutions could be tolerated at position 271 with no significant drop in activity (data not shown). In fact, this position tolerated conservative mutations such as Leu to Ile, Met or Val as well as nonconservative changes such as to Arg or Glu. This suggests minimal interactions of the side chain of 271 with the substrate, or a rather loose packing of this segment of PTE's loop 7, which is known to show high mobility (Jackson et al. 2009). The screens of both library 7-1 and 7-2 did not identify any variant with a catalytic efficiency of $>1\times10^7$ M^{-1} min^{-1} with VX or VR; however, we were able to identify variants that were more improved at VR and CVX hydrolysis relative to previous rounds.

This prompted us to systematically examine several variants along the pathway of directed evolution. Thus, we chose to examine the activities of the best variants from rounds 1, 2, 5, 6, and 7 with different OPs and compare them to those of the wt-PTE S5 starting point (Table 7). In the absence of crystal structures of these variants, sequence–activity relationships may reveal positions and substitutions that modulate PTE's catalytic efficiency.

Table 8 Mutational composition of variants selected from Round 6

Amino acid	I-F4	IV-H3	V-A4	III-D10	IID9	VF9	wt-PTES5
59	C	C	C	C	F	F	C
77	A	A	A	A	A	A	K
80	V	V	V	V	V	V	A
106	A	A	A	A	A	A	I
111	S	S	S	S	R	S	S
132	E	E	E	E	E	E	F
173	N	N	N	Q	T	T	T
203	A	A	A	F	T	D	A
208	D	D	D	D	D	D	G
233	D	D	D	D	S	T	D
254	G	G	G	G	G	G	H
266	A	A			A	A	A
270	E	E	A	A	A	A	A
274	I	I	N	N	S	S	I
342	S	P	P	P	P	P	P

Variant names are listed on the top row. Mutations in variants are listed relative to the sequence of wt-PTE S5 whose sequence is listed on the right column. Spaces denote a deleted amino acid

Specifically, by systematically varying the size and character of the leaving group, the O-alkyl moiety and the alkyl moiety of the phosphonate group, we could explore their influence on the catalytic efficiency of each variant and better understand the limits of substrate binding and hydrolysis.

Most variants were highly efficient when hydrolyzing *N*,*N*-diisopropyl substrates and were ~twofold less efficient with *N*,*N*-di-ethyl substrates and ~fivefold less efficient with *N*,*N*-di-methyl substrates (Supplementary Table 10a). This may indicate that better binding mediated by the large isopropyl moieties improves substrate hydrolysis rates relative to substrates with smaller N-alkyl groups. A noticeable exception was variant IVA1, which preferred *N*,*N*′-diethyl containing substrates such as amiton over *N*,*N*′-diisopropyl containing substrates. This may reflect an altered binding site of the *N*,*N*′-dialkyl moiety in this variant, possibly due to the D233G or Del266 mutations that are specific to IVA1.

The catalytic efficiencies of variants with substrates that differ only in the size of their alkyl phosphonate moiety (R1; Supplementary Table 10b) showed more pronounced effects. Ethyl phosphonate substrates were hydrolyzed ~threefold faster than methyl phosphonates, and between six- and 415-fold faster than O-ethyl containing substrates. The transition from phosphonate to phosphate hydrolysis can mostly explain this large reduction in activity with the exception of chlorpyrifos-oxon (Table 6). Finally, a comparison of substrates that differ only in the size of their O-alkyl group (R2; Supplementary Table 10c) revealed that large O-alkyl substrates such as those in VR and CVX are hydrolyzed with similar, or even higher rates than O-methyl substrates with the same leaving and R1 groups. This supports the notion that binding of substrates with small alkyl and O-alkyl moieties may result in a greater number of nonproductive substrate binding conformations and reduce overall catalytic efficiency (Ben-David et al. 2012).

Comparing the sequences of the examined variants (Table 7) with the fold increase in their catalytic efficiency with different substrates (Table 9) indicates that most of the improvements in activity relate to mutations at three key positions: Phe132Glu, Thr173Asn/Gln, and His254Gly. As previously discussed in (Cherny et al. 2013), the first two may be responsible for binding the choline-like moiety of V-agents, while the third one probably modulates substrate binding by changing the conformation of loop 7 and may also affect the nucleophile center by suppressing an ionic pair between His254 and D301. The contributions of other mutations such as A270E or D233G to substrate binding and catalysis are harder to infer. Comparing variants A53,

Table 9 Fold changes in catalytic efficiencies of variants relative to wt-PTE S5

Selection round	7	6	5	5	2	1	0
Substrates	IV-A1	IV-H3	C23	A53	B141	RD1-G83	wt-PTE S5
Chlorpyrifos-oxon	2	0	5	3	2	0	1
GA	0	0	0	0	0	0	1
GB	3	1	8	2	2	2	1
VE	543	281	636	159	25	9	1
Isopropyl-VE	220	144	213	125	24	4	1
VX	248	102	583	182	20	4	1
Methyl-VE	883	273	840	128	14	8	1
VM	403	115	574	114	14	2	1
GD	15	3	27	6	2	10	1
Mevinphos	0	0	2	0	1	0	1
GF	15	6	14	22	5	3	1
Dimethyl-VX	559	170	581	119	4	8	1
n-Propyl-VX	238	111	306	43	12	4	1
CVX	2542	1308	563	1542	6	10	1
VR	5856	1656	496	1544	8	11	1
Methyl-VM	160	79	104	61	2	2	1
Diisopropyl-amiton	24	21	54	8	7	5	1
Amiton	126	7	39	16	3	2	1
Dimethyl-amiton	17	17	131	12	20	5	1
Malaoxon	0	1	1	1	1	1	1

Variants are aligned by rounds of directed evolution from the wt-PTE S5 starting point—round 0 (right) to the most improved variant of round 7 (left)

IVH3, and IVA1 to C23 and to other variants indicates that position 106 is key in determining the activity on VX and VR, as previously described in (Cherny et al. 2013). Thus, Ala seems to be required at position 106 for efficient VR and CVX hydrolyzing variants, whereas efficient VX hydrolysis demands an Ile at this position. In addition, activity with VR and CVX seems to be supported by larger residues at position 59 (e.g., Phe or Met).

All PTE variants, including the wt-PTE S5, had a high catalytic efficiency (k_{cat}/K_M values $>10^7$ M^{-1} min^{-1}) with the G-type agents GA and GB (Table 5). The ability to detoxify G-agents decreased substantially with GD and GF, both alkyl-methyl-phosphonofluoridates with a bulky O-alkyl side chain, i.e., pinacolyl and cyclohexyl, respectively. These structural features indicate that in the case of G-type nerve agents, the O-alkyl substitute determines much of the catalytic efficiency of PTE variants. Overall, it seems that the size of the phosphate substituents (the R1 and R2 groups) has a much greater effect on catalytic efficiency than that of the leaving group X. Thus, correct binding of the phosphate moiety of OPs in general, and V-agents in particular, at an optimal configuration for catalysis seems to drive the largest gains in catalytic efficiency of the evolved PTE variants.

The appalling number of annual poisonings by OP pesticides with estimated up to 300,000 death per year (Gunnell et al. 2007) prompted us to investigate the ability of the PTE variants to detoxify selected pesticides. Since we used the AChE inhibition assay, the active metabolites of malathion and chlorpyrifos, i.e., malaoxon and chlorpyrifos-oxon, as well as the pesticide mevinphos, were tested. These OPs are all phosphates containing small O-alkyl R1 and R2 groups and characterized by rather bulky leaving groups. In the case of malaoxon, its leaving group is attached by a P-S bond that makes hydrolysis more difficult with respect to P-O attached leaving groups (Table 1). All PTE variants detoxified malaoxon at a rate even lower than for amiton and its analogues. Mevinphos was substantially more susceptible to detoxification by PTE variants due to its P-O leaving group bond, yet was hydrolyzed at lower rates than most V-agents. In contrast, chlorpyrifos-oxon was hydrolyzed by all the PTE variants tested at high k_{cat}/K_M values $>10^8$ M^{-1} min^{-1} (Table 6, Supplementary Table 10d.) with a k_{cat}/K_M value of 1.44×10^9 M^{-1} min^{-1} for C23. This may be due to the similarity between this pesticide and parathion, which PTE has naturally evolved to hydrolyze. Alternatively, the substituted aromatic ring of chlorpyrifos-oxon may restrict the number of binding conformations in the active site of PTE, locking the substrate into a mode that is optimized for hydrolysis by the enzyme in spite of its small O-ethyl R1 and R2 groups. It is important to note that in addition to PTE, chlorpyrifos-oxon is also hydrolyzed at a high rate by human PON1 (Eaton et al. 2008; Stevens et al. 2008).

AChE is preferentially inhibited by the toxic P(−) nerve agent enantiomers (Benschop and Dejong 1988), with the degree of stereopreference being dependent on the structure of the nerve agent, ranging from 400-fold (VX) (Reiter et al. 2008) to several thousand-fold (GD) (de Jong and Benschop 1988). By using an AChE inhibition assay, the rates of hydrolysis of the toxic P(−) enantiomers by PTE could be determined irrespective of the hydrolysis of the markedly less toxic P(+) enantiomers. The catalytic efficiencies of wt-PTE S5, as well as variants A53 and C23 with several nerve agents were previously determined both by the AChE inhibition assay and the DTNB hydrolysis assay (Cherny et al. 2013). However, the rates previously determined for these variants were up to threefold higher with most OPs tested due mainly to differences in zinc ion buffer concentrations. We found that zinc ion concentrations greater than 3 μM have an inhibitory effect on PTE activity, with the magnitude of inhibition varying between different variants (Supplementary Table 9). Indeed, while previous rates (Cherny et al. 2013) were obtained following the removal of zinc from the assay buffer of all variants, the results presented here were obtained using a buffer containing 10 μM $ZnCl_2$. The physiological concentration of zinc ions in adult plasma is estimated to be 16.6 ± 6.2 μM (Rukgauer et al. 1997). However, most of it is in protein-bound form (98 %) and the rest is in a low molecular weight ligand-bound form (1–2 %) (Takeda 2001). Thus, the concentration of free ionic zinc in plasma is estimated to be as low as 10^{-9}–10^{-10} M (Harris and Keen 1989; Magneson et al. 1987), far below the inhibitory concentration values we found in vitro. Indeed, when we tested the activity of C23 in human blood samples, we found no inhibition of activity (data not shown). Other factors were also found to influence the measured catalytic efficiencies of variants such as temperature. It was observed that at higher temperatures (e.g., 37 vs. 25 °C), the catalytic rate increased but at the expense of enzyme inactivation as well as aggregation of unstable variants. Furthermore, small differences in protein purity, handling and experimental setups can accumulate to generate differences in several folds in the measured catalytic activity.

In conclusion, using directed evolution methods, we were able to evolve a PTE variant with improved catalytic efficiencies of VR and CVX hydrolysis. Although its activity should be increased further to successfully fulfill the role of a bioscavenger for in vivo prophylaxis or post-exposure treatments using low protein doses (~1 mg/Kg), it can serve as an improved starting point for further directed evolution experiments. In the absence of structural data, we demonstrated an alternative method for deriving structure–activity-related information by profiling the activity of selected variants with structurally different substrates. While similar profiling has been done by others using nerve

agent surrogates (Bigley et al. 2013; Chen-Goodspeed et al. 2001; Tsai et al. 2010), in this work it was done using the actual threat agents. The analysis of variants selected from consecutive rounds of directed evolution highlighted the fact that increasing variant activity tends to trade-off with broad substrate specificity.

Acknowledgments The study was funded by the German Ministry of Defence. The authors wish to thank Dr. Shira Albeck from the Israel Structural Proteomics Center (ISPC), Rehovot, Israel, for the expression and purification of the PTE variants and are grateful to M. Baumann and T. Hannig for their expert technical assistance. PJG was supported by Carlsberg-fondet and EMBO Long-term postdoctoral fellowship. PTE variants were engineered and studied under a DTRA Project Grant (HDTRA1-11-C-0026),

Compliance with ethical standards

Conflict of interest The authors declare that there are no conflicts of interest.

References

Aldridge WN, Reiner E (1972) Enzyme inhibitors as substrates—interactions of esterases with esters of organophosphorus and carbamic acids. North-Holland, Amsterdam

Ashani Y, Pistinner S (2004) Estimation of the upper limit of human butyrylcholinesterase dose required for protection against organophosphates toxicity: a mathematically based toxicokinetic model. Toxicol Sci 77(2):358–367. doi:10.1093/toxsci/kfh012

Aurbek N, Thiermann H, Szinicz L, Eyer P, Worek F (2006) Analysis of inhibition, reactivation and aging kinetics of highly toxic organophosphorus compounds with human and pig acetylcholinesterase. Toxicology 224(1–2):91–99. doi:10.1016/j.tox.2006.04.030

Ben-David M, Elias M, Filippi JJ et al (2012) Catalytic versatility and backups in enzyme active sites: the case of serum paraoxonase 1. J Mol Biol 418(3–4):181–196. doi:10.1016/j.jmb.2012.02.042

Benning MM, Shim H, Raushel FM, Holden HM (2001) High resolution X-ray structures of different metal-substituted forms of phosphotriesterase from *Pseudomonas diminuta*. Biochemistry 40(9):2712–2722

Benschop HP, Dejong LPA (1988) Nerve agent stereoisomers—analysis, isolation, and toxicology. Acc Chem Res 21(10):368–374. doi:10.1021/ar00154a003

Bierwisch A, Zengerle M, Thiermann H, Kubik S, Worek F (2014) Detoxification of alkyl methylphosphonofluoridates by an oxime-substituted beta-cyclodextrin—an in vitro structure-activity study. Toxicol Lett 224(2):209–214. doi:10.1016/j.toxlet.2013.10.024

Bigley AN, Xu CF, Henderson TJ, Harvey SP, Raushel FM (2013) Enzymatic neutralization of the chemical warfare agent VX: evolution of phosphotriesterase for phosphorothiolate hydrolysis. J Am Chem Soc 135(28):10426–10432. doi:10.1021/ja402832z

Chen-Goodspeed M, Sogorb MA, Wu F, Hong SB, Raushel FM (2001) Structural determinants of the substrate and stereochemical specificity of phosphotriesterase. Biochemistry 40(5):1325–1331

Cherny I, Greisen P, Ashani Y et al (2013) Engineering V-type nerve agents detoxifying enzymes using computationally focused libraries. ACS Chem Biol. doi:10.1021/cb4004892

Das R, Baker D (2008) Macromolecular modeling with rosetta. Annu Rev Biochem 77:363–382. doi:10.1146/annurev.biochem.77.062906.171838

Dawson RM, Pantelidis S, Rose HR, Kotsonis SE (2008) Degradation of nerve agents by an organophosphate-degrading agent (OpdA). J Hazard Mater 157(2–3):308–314. doi:10.1016/j.jhazmat.2007.12.099

de Jong LPA, Benschop HP (1988) Biochemical and toxicological implications of chirality in anticholinesterase organophosphates. In: Ariens EJ, van Rensen JJS, Welling W (eds) Stereoselectivity of pesticides—biological and chemical problems. Elsevier, Amsterdam, pp 109–149

Dodge JT, Mitchell C, Hanahan DJ (1963) The preparation and chemical characteristics of hemoglobin-free ghosts of human erythrocytes. Arch Biochem Biophys 100:119–130

Eaton DL, Daroff RB, Autrup H et al (2008) Review of the toxicology of chlorpyrifos with an emphasis on human exposure and neurodevelopment. Crit Rev Toxicol 38:1–125. doi:10.1080/10408440802272158

Ellman GL, Courtney KD, Andres V Jr, Feather-Stone RM (1961) A new and rapid colorimetric determination of acetylcholinesterase activity. Biochem Pharmacol 7:88–95

Goldsmith M, Ashani Y, Simo Y et al (2012) Evolved stereoselective hydrolases for broad-spectrum G-type nerve agent detoxification. Chem Biol 19(4):456–466. doi:10.1016/j.chembiol.2012.01.017

Grob D (1956) The manifestations and treatment of poisoning due to nerve gas and other organic phosphate anticholinesterase compounds. AMA Arch Intern Med 98(2):221–239

Gunnell D, Eddleston M, Phillips MR, Konradsen F (2007) The global distribution of fatal pesticide self-poisoning: systematic review. BMC Public Health 7:357. doi:10.1186/1471-2458-7-357

Gupta RD, Goldsmith M, Ashani Y et al (2011) Directed evolution of hydrolases for prevention of G-type nerve agent intoxication. Nat Chem Biol 7(2):120–125. doi:10.1038/nchembio.510

Harris WR, Keen C (1989) Calculations of the distribution of zinc in a computer model of human serum. J Nutr 119(11):1677–1682

Jackson CJ, Foo JL, Tokuriki N et al (2009) Conformational sampling, catalysis, and evolution of the bacterial phosphotriesterase. Proc Natl Acad Sci USA 106(51):21631–21636. doi:10.1073/pnas.0907548106

Johnson MK, Jacobson D, Meredith TJ et al (2000) Evaluation of antidotes for poisoning by organophosphorus pesticides. Emerg Med 12:22–37

Kamisetty H, Ovchinnikov S, Baker D (2013) Assessing the utility of coevolution-based residue-residue contact predictions in a sequence- and structure-rich era. Proc Natl Acad Sci USA 110(39):15674–15679. doi:10.1073/pnas.1314045110

Lenz DE, Yeung D, Smith JR, Sweeney RE, Lumley LA, Cerasoli DM (2007) Stoichiometric and catalytic scavengers as protection against nerve agent toxicity: a mini review. Toxicology 233(1–3):31–39. doi:10.1016/j.tox.2006.11.066

Magneson GR, Puvathingal JM, Ray WJ Jr (1987) The concentrations of free Mg^{2+} and free Zn^{2+} in equine blood plasma. J Biol Chem 262(23):11140–11148

Marrs TC (2007) In: Marrs TC, Maynard RL, Sidell FR (eds) Chemical warfare agents: toxicology and treatment. Wiley, Chichester, pp 191–221

Masson P, Rochu D (2009) Catalytic bioscavengers: the next generation of bioscavenger-based medical countermeasures. In: Gupta RD (ed) Handbook of toxicology of chemical warfare agents. Academic Press, London, pp 1053–1065

Masson P, Carletti E, Nachon F (2009) Structure, activities and biomedical applications of human butyrylcholinesterase. Protein Pept Lett 16(10):1215–1224

Nachon F, Brazzolotto X, Trovaslet M, Masson P (2013) Progress in the development of enzyme-based nerve agent bioscavengers. Chem Biol Interact 206(3):536–544. doi:10.1016/j.cbi.2013.06.012

Reiter G, Mikler J, Hill I, Weatherby K, Thiermann H, Worek F (2008) Chromatographic resolution, characterisation and quantification of VX enantiomers in hemolysed swine blood samples. J Chromatogr B 873(1):86–94. doi:10.1016/j.jchromb.2008.08.001

Remmert M, Biegert A, Hauser A, Soding J (2012) HHblits: lightning-fast iterative protein sequence searching by HMM–HMM alignment. Nat Methods 9(2):173–175. doi:10.1038/nmeth.1818

Rockah-Shmuel L, Tawfik DS, Goldsmith M (2014) Generating targeted libraries by the combinatorial incorporation of synthetic oligonucleotides during gene shuffling (ISOR). Methods Mol Biol 1179:129–137. doi:10.1007/978-1-4939-1053-3_8

Roodveldt C, Tawfik DS (2005) Directed evolution of phosphotriesterase from *Pseudomonas diminuta* for heterologous expression in *Escherichia coli* results in stabilization of the metal-free state. Protein Eng Des Sel 18(1):51–58. doi:10.1093/protein/gzi005

Rukgauer M, Klein J, Kruse-Jarres JD (1997) Reference values for the trace elements copper, manganese, selenium, and zinc in the serum/plasma of children, adolescents, and adults. J Trace Elem Med Biol 11(2):92–98. doi:10.1016/S0946-672X(97)80032-6

Stevens RC, Suzuki SM, Cole TB, Park SS, Richter RJ, Furlong CE (2008) Engineered recombinant human paraoxonase 1 (rHuPON1) purified from Escherichia coli protects against organophosphate poisoning. Proc Natl Acad Sci USA 105(35):12780–12784. doi:10.1073/pnas.0805865105

Takeda A (2001) Zinc homeostasis and functions of zinc in the brain. Biometals 14(3–4):343–351

Thiermann H, Worek F, Kehe K (2013) Limitations and challenges in treatment of acute chemical warfare agent poisoning. Chem Biol Interact 206(3):435–443. doi:10.1016/j.cbi.2013.09.015

Tsai PC, Bigley A, Li Y et al (2010) Stereoselective hydrolysis of organophosphate nerve agents by the bacterial phosphotriesterase. Biochemistry 49(37):7978–7987. doi:10.1021/bi101056m

Worek F, Thiermann H (2013) The value of novel oximes for treatment of poisoning by organophosphorus compounds. Pharmacol Ther 139(2):249–259. doi:10.1016/j.pharmthera.2013.04.009

Worek F, Mast U, Kiderlen D, Diepold C, Eyer P (1999) Improved determination of acetylcholinesterase activity in human whole blood. Clin Chim Acta 288(1–2):73–90. doi:10.1016/S0009-8981(99)00144-8

Worek F, Seeger T, Goldsmith M et al (2014a) Efficacy of the rePON1 mutant IIG1 to prevent cyclosarin toxicity in vivo and to detoxify structurally different nerve agents in vitro. Arch Toxicol 88(6):1257–1266. doi:10.1007/s00204-014-1204-z

Worek F, Seeger T, Reiter G et al (2014b) Post-exposure treatment of VX poisoned guinea pigs with the engineered phosphotriesterase mutant C23: a proof-of-concept study. Toxicol Lett 231(1):45–54. doi:10.1016/j.toxlet.2014.09.003